Bioconjugate Chemistry

Article

pubs.acs.org/bc

Universal Antibody Conjugation to Nanoparticles Using the Fcγ Receptor I (FcγRI): Quantitative Profiling Of Membrane Biomarkers

Chloe Kim,[†,‡] Justin F. Galloway,[†,‡] Kwan Hyi Lee,[‡,§] and Peter C. Searson*[,†,‡]

[†]Department of Materials Science and Engineering and [‡]Institute for Nanobiotechnology, Johns Hopkins University, 3400 North Charles Street, Baltimore, Maryland 21218, United States

[§]KIST Biomedical Research Institute, 5 Hwarangno 14-gil, Seongbuk-gu, Seoul 136-791, Korea

Supporting Information

ABSTRACT: Antibodies are a class of molecules widely used in bioengineering and nanomedicine for applications involving protein recognition and targeting. Here we report an efficient method for universal conjugation of antibodies to lipid-coated nanoparticles using radially oriented FcγRIs. This method is performed in physiological solution with no additional coupling reagents, thereby avoiding problems with antibody stability and functionality. Coupling to the Fc region of the antibody avoids aggregation and polymerization allowing high yield. In addition, the antibody is oriented perpendicular to the surface so that the binding sites are fully functional. Using this method we demonstrate quantitative profiling of a panel of four membrane-bound cancer biomarkers (claudin-4, mesothelin, mucin-4, and cadherin-11) on four cell lines (Panc-1, MIA PaCa-2, Capan-1, and HPDE). We show that by designing the lipid coating to minimize aggregation and nonspecific binding, we can obtain absolute values of biomarker expression levels as number per unit area on the cell surface. This method is applicable to a wide range of technologies, including solution based protein detection assays and active targeting of cell surface membrane biomarkers.

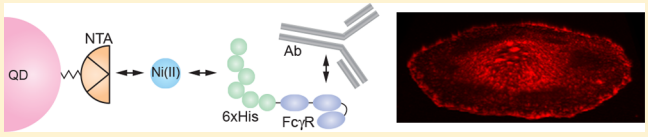

The ability to reliably and reproducibly conjugate antibodies to nanoparticles is key to developing platforms for next generation technologies from diagnostics to therapeutics.[1] Applications include single molecule tracking, cell sorting, bioseparations, quantitative assays for protein detection, enzyme immobilization, protein purification, immunoasays, along with *in vivo* applications such as targeted contrast agents for imaging and targeted drug/gene delivery.[1−12]

Monoclonal antibodies (mAbs) are widely used for protein recognition and targeting since they have two epitope binding sites, high selectivity, and high binding affinity.[5] Despite the efforts devoted to the development of antibody-conjugated nanoparticles, there remain many challenges and limitations.[9] Conventional approaches generally involve modification of the nanoparticle surface with reactive groups, such as carboxyl or amine groups, that can be covalently coupled to a side group on a surface residue of the antibody using standard bioconjugation methods (e.g., EDC/NHS chemistry).[7] These covalent coupling methods have several drawbacks, including (1) aggregation and polymerization due to cross-linking at multiple sites on the antibody, (2) additional purification steps needed to remove cross-linking and catalytic reagents that result in low yield and poor reproducibility, and (3) random orientation of the antibody on the nanoparticle surface such that the antigen binding sites may not be accessible. Several noncovalent coupling methods have also been explored for antibody conjugation. The most promising involve functionalization of the nanoparticle surface with immunoglobulin binding proteins, such as protein A and protein G,[13,14] or by coupling biotinylated antibodies to an avidin modified particles.[15]

Here we use FcγRIs for antibody conjugation to a nanoparticle surface (Figure 1A). This approach has several advantages: (1) antibody conjugation is performed in physiological solution with no additional coupling reagents, thereby avoiding the necessity for additional purification steps and problems with antibody stability and functionality; (2) coupling to the Fc region of the antibody by the FcγRI avoids aggregation and polymerization allowing high yield; (3) the antibody is oriented perpendicular to the surface such that the binding sites are fully functional; and (4) antibodies can be used interchangeably. The FcγRIs and antibodies are conjugated to quantum dots (QDs) for optical detection. Fluorescence-based methods are widely used for biomarker identification and determination of relative expression levels; however, photobleaching of organic fluorophores severely limits quantitative analysis. QDs exhibit stable and tunable emission, enabling applications requiring single molecule tracking, quantitative analysis, and multiplexing.[7,12,14,16]

The Fc receptors (FcRs) are a class of cell-surface molecules that bind to the Fc region of antibodies and facilitate efficient antibody−antigen interactions. In humans, about 75% of antibodies in the circulation are immunoglobulin-Gs (IgGs): antibodies with two identical heavy chains and two identical light chains arranged in a characteristic Y-shape. Receptors for the Fc

Received: August 14, 2014
Revised: September 12, 2014
Published: September 12, 2014

   dx.doi.org/10.1021/bc5003778 | *Bioconjugate Chem.* 2014, 25, 1893−1901

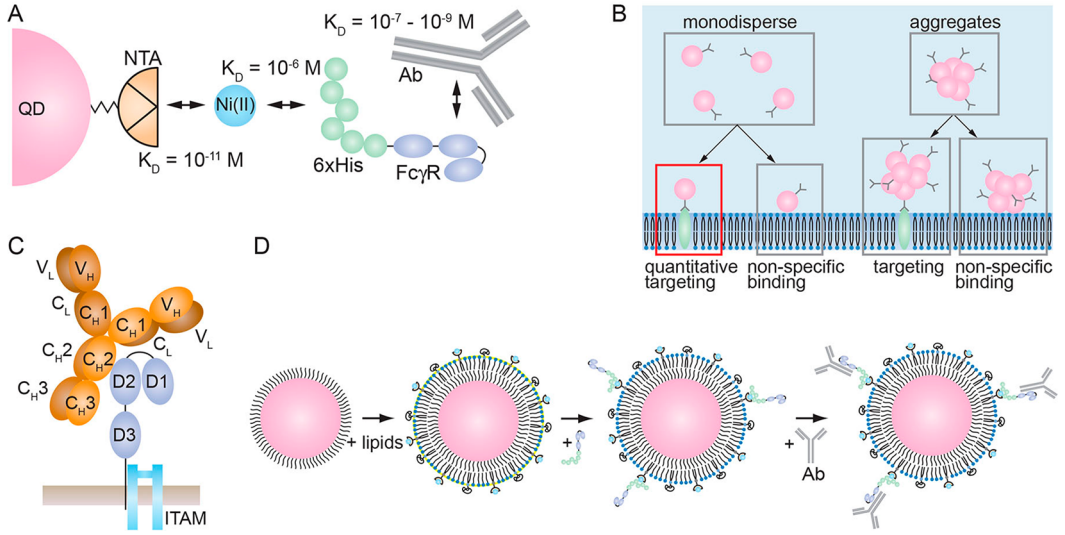

Figure 1. Strategy for universal antibody conjugation to nanoparticles using Fcγ receptor I (FcγRI). (A) Schematic illustration of antibody conjugation to lipid coated QDs using FcγRI. The binding affinities (dissociation constants) are 10^{-11} M (NTA - Ni(II)), 10^{-6} M (Ni(II) - histag), and 10^{-7}–10^{-9} M (FcγRI - IgG). (B) The main requirements for quantitative detection of biomarker expression at the cell surface are one probe (QD-Ab conjugate) per cell surface biomarker, minimal aggregation, negligible nonspecific binding, and saturation of all cell surface biomarkers. (C) Structurally, FcγRI receptors have three extracellular domains and an associated immunoreceptor tyrosine activation motif (ITAM). The FcγRI binds to the heavy chain region of IgG antibodies orienting the antigen binding sites perpendicular to the surface. (D) QD functionalization involves the formation of an outer lipid layer on the core/shell QD with native hydrophobic surfactants. The lipids include a single acyl chain lipid, a double acyl chain lipid with a PEG group, and a double acyl chain phospholipid with a nitrolotriacetic acid (NTA) moiety attached to the headgroup. FcγRIs with a histag are coupled to the Ni(II)/NTA groups and antibodies are coupled to the FcγRIs. Antibodies conjugated to the FcγRIs are oriented perpendicular to the surface to ensure that the antigen binding sites are active.

region of IgGs are known as FcγRs and are involved in immune responses such as cell activation and inhibition, phagocytosis, antibody-dependent cell mediated toxicity (ADCC), cytokine release, and B cell proliferation.[17−20]

The FcγRs are divided into three classes: FcγRI (CD64), FcγRII (CD32), and FcγRIII (CD16).[17−19] The FcγRI (CD64) has an affinity of 10^{-7}–10^{-9} M to monomeric IgG (10^{-7}–10^{-8} M for mouse IgG), significantly higher than FcγRII and FcγRIII which have binding affinities of 10^{-6}–10^{-7} M.[21] The high affinity recognition of IgG by FcγRI permits the triggering of effector responses at low IgG concentrations typical of early immune responses. FcγRI is expressed constitutively on monocytes and macrophages and can be induced on neutrophils and eosinophils.[20,21] Structurally, the extracellular region of FcγRI has three Ig-like domains, which allows high affinity binding to a single antibody.[17−19] Domains D1 and D2 are joined at an acute angle, which is maintained by a network of hydrogen bonds, and the ligand-binding sites of are located in domain 2 (Figure 1C).[18] Therefore, we have selected the FcγRI for universal conjugation since it has high affinity to the Fc region of a single antibody, allowing a 1:1 ratio for FcγRI/antibody binding. The FcγRI has several advantages over other binding proteins for antibody conjugation. For example, protein A has five binding sites for the Fc region of IgGs and protein G has two binding sites.[22−24] In addition, although protein A and protein G have strong binding affinity for human IgGs, protein G has moderate affinity and protein A has weak affinity for mouse IgGs commonly used in research.[22−24]

To demonstrate universal antibody conjugation using FcγRIs, we report on quantitative targeting of a panel of four membrane-bound cancer biomarkers (claudin-4, mesothelin, mucin-4, and cadherin-11) on four cell lines (Panc-1, MIA PaCa-2, Capan-1, and HPDE). The relative expression levels for some of the biomarker/cell line combinations are known (see Supporting Information Figure S1), allowing qualitative comparison to our method for universal antibody conjugation. In addition, we report new results on the quantitative expression levels of mucin-4 and cadherin-11 on the four cell lines.

RESULTS AND DISCUSSION

QD-FcR-Ab Characterization. To conjugate the FcγRI to the lipid-modified QDs, we use a Ni(II)-NTA complex/his-tag motif (Figure 1A). The complexation of divalent transition metals to a chelator such as nitrolotriacetic acid (NTA) is widely used for protein purification.[25] To incorporate the NTA group into the lipid layer on the nanoparticle, we use a commercially available double acyl chain phospholipid with a NTA group appended to the headgroup (DOGS-NTA-Ni) (Figure 1A). The FcγRI is coupled to the Ni(II)-NTA complex using a his-tag with six histidine residues. An FcγRI with a 6xHis-tag coupled to the C-terminus is commercially available. While FcγRIs could be attached to a lipid coated nanoparticle by synthesizing a fusion protein with a transmembrane domain that inserts into the lipid layer, all lipids and reagents in our approach are commercially available thereby avoiding the need for specialized synthesis methods.

The dissociation constant for the Ni(II)-NTA complex is 10^{-11} M,[25] and for the Ni(II)–6xHis-tag is 10^{-6} M (Figure 1A).[25] As described previously, the dissociation constant for FcγRI-IgG binding is 10^{-7}–10^{-9} M for human FcγRI and 10^{-7}–10^{-8} M for mouse FcγRI.[19] In protein purification, the difference in K_d between the Ni(II)-NTA complex and the Ni(II)–6xHis-tag interaction is exploited in stripping and regeneration. For example, imidazole (K_d = 10^{-3} M for imidazole-Ni(II)) is used for protein elution whereas EDTA (K_d = 10^{-19} M for EDTA-Ni(II)) is used for regeneration.[25] The dissociation constants for antibody–antigen binding varies over a wide range from 10^{-6} to

dx.doi.org/10.1021/bc5003778 | Bioconjugate Chem. 2014, 25, 1893−1901

10^{-9} M, but can be as high as 10^{-12} M for high affinity antibodies.[26]

The QDs are water solubilized by forming a lipid layer on the surface (Figure 1D).[16,27−29] Lipid encapsulation is relatively straightforward, taking advantage of the native hydrophobic surfactants on the QD surface after synthesis to drive the formation of an outer layer of amphiphilic lipids, analogous to the outer leaflet in a cell membrane. The combination of the outer lipid layer and the inner layer of hydrophobic surfactants provides stability and protects the QD core. Many lipids are commercially available, including those with single and double acyl chains, head groups with ligands that can be used for covalent conjugation, and pegylated lipids, providing significant flexibility in designing lipid coatings with multiple components for specific applications.

The lipid coated QDs in water showed an average hydrodynamic diameter of 15.7 ± 3 nm (Figure 2A). The average

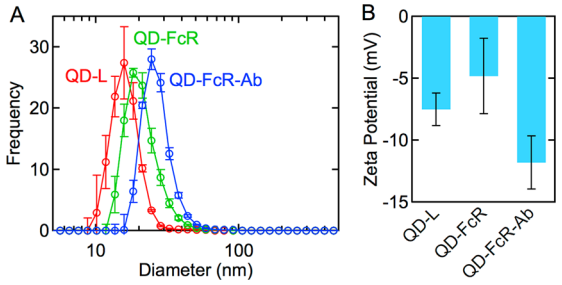

Figure 2. Characterization of QD-FcR-Ab conjugates. (A) Particle size distribution for lipid conjugated QDs (QD-L), lipid-conjugated QDs after incorporation of the his-tag FcR (QD-FcR), and after antibody coupling (QD-FcR-Ab). (B) Zeta potential for QD conjugates.

diameter of the core/shell QDs is about 8 nm.[27] Taking a thickness of 1 nm for the HDA/TOPO inner leaflet and a thickness of 2 nm for the outer leaflet, we would expect a diameter of about 14 nm for lipid coated QDs without additional functional groups. The hydrodynamic size of PEG2k on the DSPE-PEG2k phospholipid is 2 nm,[27] and hence a lipid-coated nanoparticle with a complete monolayer of PEG2k at the surface would be expected to have a diameter of 18 nm. Here we use 10 mol % DSPE-PEG2k so that the PEG2k groups, assuming a footprint of 4 nm^2, correspond to a coverage of about 55%. Therefore, the measured diameter of 16 nm is intermediate between 0% and 100% PEG2k (14−18 nm).

The addition of the three FcγRIs per QD resulted in an increase of size from 15.7 to 18.2 nm (Figure 2A). Conjugation with three antibodies resulted in an increase in hydrodynamic diameter to 24.4 ± 1.7 nm. A typical antibody (150 kDa) is about 15 nm long and about 5 nm in diameter at the base, and hence the FcγRI receptor (35 kDa) is expected to be about 5 nm in length. Therefore, the increase in hydrodynamic size is consistent with the addition of a small number of FcR groups and antibodies.

The zeta potential for the lipid-coated QDs with 80 mol % MHPC, 10 mol % DSPE-PEG2K, and 10 mol % DOGS-NTA-Ni was about −7.5 mV (Figure 2B). In previous work we reported a similar zeta potential of about −9 mV for QDs functionalized with an outer leaflet of MHPC and 10−50 mol % DSPE-PEG2k.[27] The addition of the Fc-receptor resulted in negligible change in zeta potential (Figure 2B). The final zeta potential, after conjugation with anti-CLDN4, was −11.8 mV. Since the isoelectric point for IgG1 monoclonal antibodies is 6.6−7.1,[30] they are expected to be negatively charged, and hence the zeta potential is expected to show a small decrease.

For any conjugation scheme, the overall yield can be important in cost and utilization of reagents. Figure 3 shows the fraction of

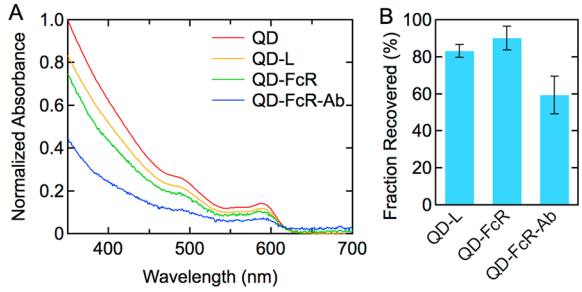

Figure 3. Yield during surface modification. (A) Absorbance spectra for QDs in chloroform (QD) and QD conjugates during surface modification, normalized to the initial concentration in chloroform. (B) Fraction of QDs recovered after surface modification steps. Determined from absorbance measurements (see Materials and Methods for details).

QDs recovered (see Materials and Methods) after each step. After the initial lipid coating and water solubilization step, the fraction of QDs in suspension was 83%, significantly higher than the yield for water-solubilization with MHPC and DSPE-PEG2k,[27] indicating that the DOGS-NTA-Ni significantly improves the stability. After conjugating with the Fc-receptor, the yield was 90%, and after antibody conjugation the yield was 59%. Therefore, the overall yield in producing QD-FcR-Ab conjugates starting with a batch of QDs in chloroform was 44%. The overall yield is relatively high, especially given the stringent requirements of antibody conjugation and monodispersity required for quantitative targeting.

Quantitative Targeting. The three main requirements for quantitative detection of biomarker expression at the cell surface are (1) one probe per surface biomarker, (2) saturation of all cell surface biomarkers, and (3) negligible nonspecific binding (Figure 1B). The requirement for a single probe (QD-Ab conjugate) per target molecule implies a monodisperse suspension with minimal aggregation, as shown in Figure 2A. To verify that all biomarkers on the cell surface are saturated, QDs were conjugated with anticlaudin-4 (aCLDN4) and the QD-FcR-aCLDN4 conjugates incubated with Panc-1 cells at a concentration of 3×10^6 to 9×10^7 QDs per cell. All cells showed relatively uniform fluorescence, with an intensity that was dependent on the concentration of the QD-FcR-aCLDN4 conjugates (Figure 4A). The background fluorescence intensity away from the cells showed no significant differences compared to experiments where cells were not incubated with the QDs, which suggests minimum nonspecific binding.

To convert the fluorescence intensity on the cell surface to the number of QDs per unit area, we performed calibrations for each batch of QDs (see Materials and Methods for details) (Figure 4B). The calibration curve (Figure 4C) is linear with a slope of one as expected for a uniform distribution of monodispersed QDs, and the intercept is dependent on the quantum yield and hence varies from batch to batch of QDs. For the experiments reported here the quantum yield of the QD-FcR-Ab conjugates varied from 30% to 44%, resulting in a maximum difference in the intercept of the calibration curves of a factor of 1.49. From the background intensity, the resolution corresponds to an expression level of about 10 μm^{-2}.

dx.doi.org/10.1021/bc5003778 | Bioconjugate Chem. 2014, 25, 1893−1901

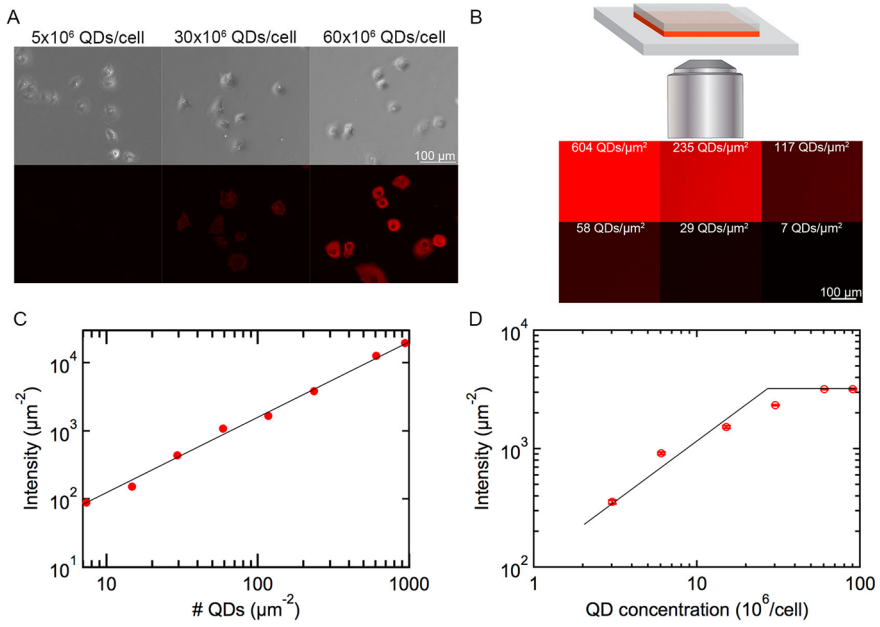

Figure 4. Quantitative cell targeting using QD-FcR-Ab conjugates. (A) phase and fluorescence images of Panc-1 cells incubated with different concentrations of QD-FcR-aCLDN4 conjugates. (B) The fluorescence of known concentrations of QD suspensions is used for calibration (see Materials and Methods for details). (C) Calibration curve showing average fluorescence intensity per unit area versus QD concentration per unit area. The calibration curve is used to convert the fluorescence intensity per unit area on the cell surface to an expression level per unit area. (D) Average fluorescence intensity per unit area for CLDN4 expression on Panc-1 cells versus QD concentration. Error bars represent standard error. Each point represents the average intensity from at least 200 cells.

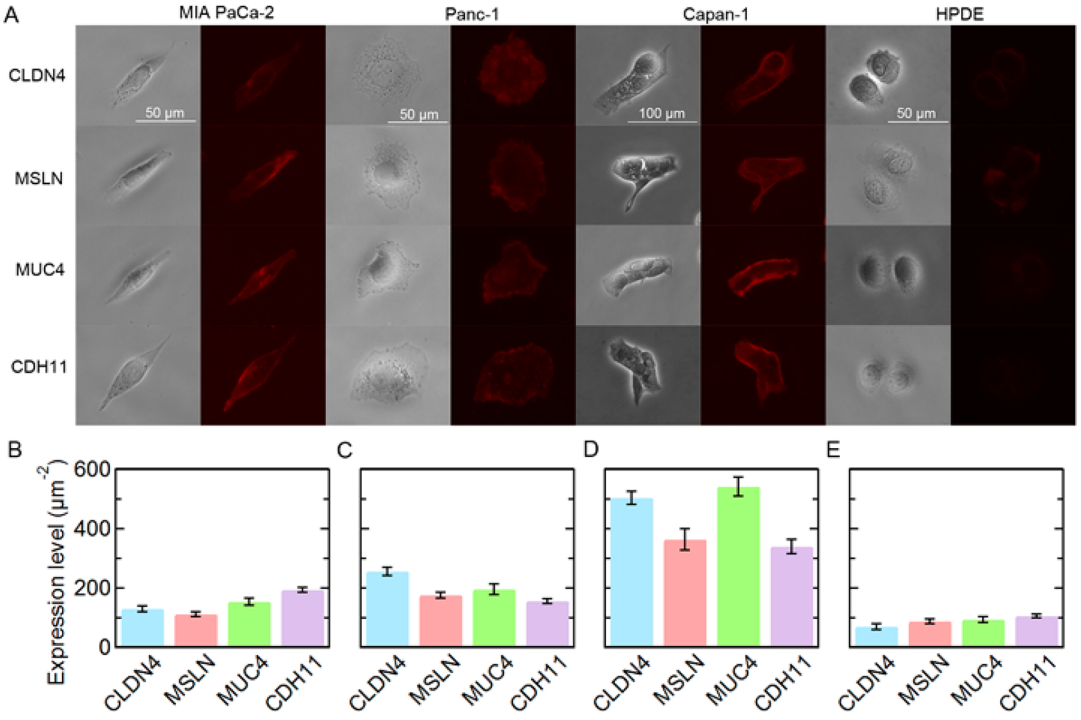

Figure 5. Quantitative expression levels for CLDN4, MSLN, MUC4, and CDH11 on Panc-1, MIA PaCa-2, Capan-1, and HPDE cells. (A) phase and fluorescence images of MiaPaCa-2, Panc-1, Capan-1, and HPDE cells incubated with QD-FcR-Ab conjugates (Ab = aCLDN4, aMSLN, aMUC4, and aCDH11). Biomarker expression levels on (B) MIA PaCa-2, (C) Panc-1, (D) Capan-1, and (E) HPDE cells. Error bars represent standard error. Expression levels for each biomarker on MIA PaCa-2, Panc-1, and HPDE are obtained from measurements of between 565−997 individual cells (see Supporting Information Figure S2 for details). For Capan-1, expression levels are based on measurements of at least 180 clusters of cells. In total, measurements were made on more than 9600 individual cells and more than 780 cell clusters.

The fluorescence intensity obtained from images of cells incubated with QD-FcR-aCLDN4 conjugates (Figure 4D) can be converted to an absolute expression level of number per square micron on the cell surface using the calibration curve (Figure 4C). For Panc-1 cells incubated with QD-FcR-aCLDN4 conjugates, the expression level initially increases linearly with

dx.doi.org/10.1021/bc5003778 | Bioconjugate Chem. 2014, 25, 1893−1901

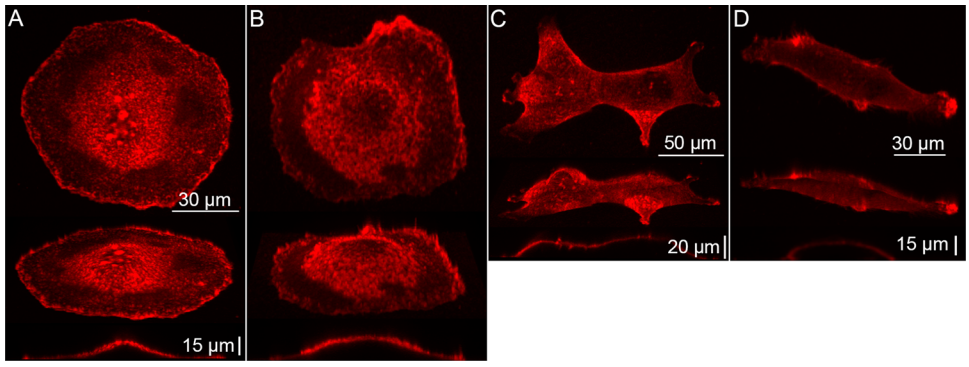

Figure 6. Confocal *z*-stack images of Panc-1 cells incubated with (A) QD-FcR-aCLDN4 and (B) QD-FcR-aMUC4 conjugates. Confocal *z*-stack images of (C) Capan-1 and (D) MIA PaCa-2 cells incubated with QD-FcR-aCLDN4 conjugates. (Top) top view, (middle) isometric view, (bottom) cross-section.

QD concentration and then saturates at an expression level of about 230 μm^{-2}. The linear region with a slope of one provides evidence that there is one QD per biomarker on the cell surface. As we describe below in more detail, preblocking of the target protein with free antibodies resulted in no detectable binding, indicating negligible nonspecific binding. For the experimental conditions used here, saturation occurred at a concentration of about 4×10^7 QDs per cell. For all subsequent experiments, we used a QD concentration of 2×10^8 QDs per cell, allowing for measurement of expression levels up to 1000−2000 μm^{-2}, close to the upper limit defined by steric exclusion. For a 25 nm QD-FcR-Ab conjugate, steric exclusion is expected to occur at a concentration of about 1600 μm^{-2}. The lower limit is dependent on many factors, including the quantum yield of the QDs, autofluorescence of the cell line, and the microscope and imaging conditions. Using a conventional fluorescence microscope, a resolution of about 10 μm^{-2} is typical.

The linkages in our QD-FcR-Ab conjugates have different binding affinities. The Ni(II)-histag linkage is the weakest with a binding constant of about 10^{-6} M. Our targeting experiments show that this linkage is stable in the experimental conditions used here for targeting in cell culture. Further evidence is provided by the fact that we can elute the QDs from the fixed cells by incubation in imidazole. Increases in the stability of this linkage could be achieved by using multivalent NTA groups.[31,32]

Profiling of Pancreatic Cancer Biomarkers. Having verified targeting using our QD-FcR-aCLDN4 conjugates, we determined the expression levels for a panel of four membrane biomarkers (CLDN4, MSLN, MUC4, and CDH11) on four cell lines (MIA PaCa-2, Panc-1, Capan-1, HPDE) (Figure 5). MIA PaCa-2 is an epithelial cell line of pancreatic cancer,[33,34] the Panc-1 cell line was established from a human pancreatic ductal adenocarcinoma,[35] and the Capan-1 cell line was established from a liver metastasis of a grade II pancreatic adenocarcinoma.[36] The immortalized pancreatic cell line HPDE (human pancreatic duct epithelium) was used as a control.[37] For some of the biomarker/cell combinations, the relative expression level is known from Western blot or other measurements, whereas in other cases the expression level is not known (see Supporting Information Figure S1).[38−42]

Claudin-4 (CLDN4). Claudin-4 is one of a large family of tight junction membrane proteins that is overexpressed in ovarian, breast, prostate, and pancreatic tumors.[38,43−47] In pancreatic cancer, the onset of claudin-4 overexpression is observed in PanIN-2 lesions.[44] Claudin-4 is weakly expressed or absent in all normal pancreas and chronic pancreatitis tissues, but is strongly overexpressed in primary and metastatic pancreatic cancer tissues.[38,44] From analysis of protein expression using Northern blot analysis, CLDN-4 was found to be expressed in 15 of 16 pancreatic cancer cell lines, with expression levels for the cell lines studied here in the order Capan-1 > Panc-1 > MIA PaCa-2.[38]

Targeting experiments with QD-FcR-Ab conjugates revealed average claudin-4 expression levels of 70 μm^{-2} on HPDE cells, 130 μm^{-2} on MIA PaCa-2 cells, 256 μm^{-2} on Panc-1 cells, and 504 μm^{-2} on Capan-1 cells (Figure 5). Expression levels for Panc-1, MIA PaCa-2, and HPDE cells were obtained from isolated, individual cells. In contrast, individual Capan-1 cells did not adhere to the surface of the dish but formed clusters. The expression levels reported here (Figure 5) are in agreement with the relative order of expression levels reported in the literature,[38] and with previous measurement of claudin-4 expression on the four cell lines using EDC-coupling to conjugate antibodies to QDs.[16] The distribution of the average expression levels per cell is relatively narrow (Figure 5C); for example, the expression level of claudin-4 on Panc-1 cells is 256 ± 13.3 μm^{-2} (SE).

Mesothelin (MSLN). Mesothelin is a cell surface glycoprotein overexpressed in ovarian and pancreatic cancers, and in mesotheliomas.[39,40,48] Immunostaining studies of tissue sections have shown that mesothelin is overexpressed in pancreatic adenocarcinomas, but is not detected in normal tissue.[49] Western blot analysis has shown MSLN expression in the order Capan-1 > Panc-1, MIA PaCa-2 > HPDE.[39] Analysis of gene expression using RT-PCR has shown strong mesothelin mRNA expression in Capan-1 cells, weak expression in Panc-1 and HPDE cells, and no detectable expression in MIA PaCa-2 cells.[40]

The expression level of mesothelin using QD-FcR-Ab conjugates was found to be 363 μm^{-2} for Capan-1, 176 μm^{-2} for Panc-1, 111 μm^{-2} for MIA PaCa2, and 88.1 μm^{-2} for HPDE (Figure 5). The strong expression levels for Capan-1 are in agreement with both protein and gene analysis reported in the literature,[39,40] and order of expression levels is in agreement with Western blot analysis.[39] The main difference between our results and gene expression is for MIA PaCa-2 cells, where we find expression levels slightly higher than HPDE cells.

Mucin-4 (MUC4). The mucins are a family of high molecular weight glycoproteins that are widely overexpressed in epithelial cells. Mucin-4 is overexpressed in pancreatic cancer,[41,42,48,50,51] and previous studies have demonstrated differential expression of MUC4 in invasive pancreatic adenocarcinoma and the absence of MUC4 in normal pancreas by RT-PCR and immunohistochemical analysis.[42] MUC4 mRNA was reported to be expressed in

75% of pancreatic adenocarcinoma tissue samples and pancreatic adenocarcinoma tumor cell lines, in 0% chronic pancreatitis and normal pancreas tissues.[41] Analysis of gene expression using RT-PCR has shown very strong expression levels in Capan-1, and undetectable levels in Panc-1 and MIA PaCa-2 cells.[41,42]

The expression levels of MUC4 were 542 μm^{-2} in Capan-1 cells, 196 μm^{-2} in Panc-1 cells, 154 μm^{-2} in MIA PaCa-2 cells, and 94 μm^{-2} in HPDE cells (Figure 5). In contrast to gene expression studies,[41,42] we observe moderate protein expression in Panc-1 and MIA PaCa-2 cells.

Cadherin-11 (CDH11). Cadherins constitute a family of transmembrane glycoproteins involved in Ca^{2+}-dependent cell−cell interactions.[52] Microarray analysis, RT-PCR, and immunohistochemistry have shown high expression levels of cadherin-11 in the stromal compartment of both pancreatic adenocarcinoma and chronic pancreatitis.[53,54] There are no qualitative or quantitative reports of cadherin-11 expression in pancreatic cancer cell lines studied here.

Our targeting results (Figure 5) also show higher expression levels of CDH11 in the cancer cell lines compared to the normal pancreatic cell line, HPDE. The expression levels of CDH11 were 339 μm^{-2} in Capan-1 cells, 155 μm^{-2} in Panc-1 cells, 194 μm^{-2} in MIA PaCa2 cells, and 106 μm^{-2} in HPDE cells (Figure 5).

Confocal Imaging. Panc-1, Capan-1, and MIA PaCa-2 cells were labeled with selected antibodies for confocal imaging (Figure 6). The confocal images of Panc-1 cells (Figure 6A,B) show a characteristic pancake-like morphology with a central approximately hemispherical nucleus. Panc-1 cells are typically 80−100 μm wide and 15−20 μm tall above the nucleus. Epifluorescence images (Figure 5) generally show uniform fluorescence over most of the cell but lower fluorescence near the nucleus where the membrane is above the focal plane. The confocal images reveal relatively uniform expression over the cell surface. Pancreatic cancer cell lines exhibit heterogeneity from cell line to cell line. Figure 6C shows confocal images of Capan-1 cells that are labeled with QD-FcR-aCLDN4. Capan-1 cells are known to form spheroids consisting of smaller cell aggregates.[55] After 3 days in culture, each cluster of Capan-1 cells contained 50 to 200 cells. Figure 6D shows confocal images of MIA PaCa-2 cells that are labeled with QD-FcR-aCLDN4. MIA PaCa-2 cells are known to be poorly differentiated and exhibit poorly developed membrane structures.[55]

Controls. To confirm our targeting results, we followed standard antibody labeling protocols to stain Panc-1 cells with CLDN4, MSLN, MUC4, and CDH11 antibodies. Immunofluorescence images (Supporting Information Figure S4) show uniform expression over the cell surface for all four antibodies with relative expression levels consistent with the quantitative results shown in Figure 5. The stable fluorescence from the QDs allows quantitative analysis, whereas photobleaching of the fluorophore makes quantitative analysis extremely difficult.

To verify that nonspecific binding of QDs was negligible, we performed blocking experiments where Panc-1 cells were first incubated with free anti claudin-4 for 30 min prior to introducing QD-FcR-aCLDN4 conjugates (Supporting Information Figure S5). The fluorescence on cells incubated with QD-FcR-aCLDN4 conjugates after preincubation with the free antibody was not detectable above the background intensity, providing evidence that the QD-FcR-Ab conjugates are specifically binding to the target protein and that nonspecific binding is negligible. We also performed control experiments where Panc-1 cells were incubated with QD-lipid and QD-FcR conjugates (no antibody) (Supporting Information Figure S5). Images for cells incubated with QD-lipid or QD-FcR conjugates revealed a small amount of punctate nonspecific staining. While the controls with QD-lipid or QD-FcR conjugates are not representative of the QD-FcR-Ab structure since the antibody provides significant steric screening (Supporting Information Figure S6), quantitative analysis of fluorescence images showed very low levels of nonspecific binding (Supporting Information Figure S7).

Reproducibility. The targeting results summarized in Figure 5 were obtained from five independent experiments (see Supporting Information Figure S2). These experiments used two different batches of QDs with quantum yields of 49% and 54% for lipid coating and functionalization. Here we compare the independent experiments for claudin-4 expression on Panc-1 cells. The average expression level of claudin-4 on Panc-1 cells from all experiments was 256 ± 13.3 μm^{-2}. Experiments #1 and #2 were performed with the same batch of core/shell-QDs but the functionalization was performed independently. The expression level for CLDN4 on Panc-1 cells was 235 μm^{-2} in Experiment #1 and 273 μm^{-2} in Experiment #2, showing good reproducibility between independent surface functionalizations. In Experiment #3, QDs were prepared from a different batch of QDs resulting in an expression level of 263 μm^{-2}, very close to the values obtained from Experiments #1 and #2. Experiments #4 and #5 were performed using the same batch of QDs and from the same surface functionalization. The CLDN4 expression levels were 218 μm^{-2} and 291 μm^{-2}, respectively. The difference in the average expression level between the minimum and maximum values was 25.1%. In the targeting experiments on Panc-1 cells, the passage numbers were between passage 3 and passage 10; however, there was no correlation between expression level and passage number over the range studied here. These results demonstrate good reproducibility between different batches of QDs and between different functionalizations.

■ CONCLUSIONS

We have demonstrated an efficient method for universal conjugation of antibodies to lipid-coated nanoparticles using a radially oriented Fcγ receptor I. This method has several advantages over conventional covalent coupling methods, including: (1) antibody conjugation is performed in physiological solution with no additional coupling reagents, thereby avoiding the necessity for additional purification steps and problems with antibody stability and functionality; (2) coupling to the Fc region of the antibody avoids aggregation and polymerization allowing high yield; (3) the antibody is oriented perpendicular to the surface so that the binding sites are fully functional; (4) antibodies can be used interchangeably; (5) the FcγRI has high affinity to the Fc region of a single antibody, allowing a 1:1 ratio for FcγRI/antibody binding, particularly important for quantitative recognition and targeting; (6) all lipids and reagents are commercially available; and (7) the yield for preparation of QD-FcR-Ab conjugates is high. Furthermore, we have shown good reproducibility between different batches of quantum dots and different surface functionalizations. This method is applicable to a wide range of technologies, including solution based protein detection assays and active targeting of cell surface membrane biomarkers.

Protein expression levels obtained using our QD-FcR-Ab conjugates for claudin-4 and mesothelin expression on Capan-1, MIA PaCa-2, and Panc-1 cells are in good agreement with the relative expression levels reported in the literature. The

expression levels for claudin-4, mesothelin, mucin-4, and cadherin-11 on Capan-1 cells of 340−550 μm^{-2}, significantly higher than the expression levels of these proteins in the other cell lines studied. Expression levels for the four proteins on Panc-1 and MIA PaCa-2 cells varied between 110 and 260 μm^{-2}, while expression levels on HPDE cells were between 70 and 110 μm^{-2}. Here we have demonstrated quantitative profiling in cell culture using QD-FcR-Ab conjugates. This method can be easily adapted for multiplexed profiling using different color QDs.

MATERIALS AND METHODS

QD Synthesis and Lipid Functionalization. CdSe cores were synthesized from CdO and Se in TOPO and HDA and passivated with a (Cd,Zn)S shell, as described previously.[27] The core/shell QDs have an average diameter of 8 nm and an emission peak at about 605 nm.[27,56] The details of lipid functionalization are provided in the Supporting Information.

FcγRI and Antibody Conjugation. Antibodies were conjugated to the lipid coated QDs using an FcγRI group attached to a his-tag. Recombinant mouse FcγRI/CD64 (R&D Systems, cat# 2074-FC-050) with a C-terminal 6xHis-tag constituted at 500 $\mu g\ mL^{-1}$ in sterile PBS was added to NTA(Ni)-terminated QDs for 30 min at RT. The concentration of the 6xHis-tag Fc-receptor was calculated to give three Fc-receptors per QD. The resulting solution was passed through a syringe filter with a 200 nm polytetrafluoroethylene membrane to remove any aggregates.

Targeting experiments were performed by conjugating antibodies of four pancreatic cancer biomarkers:[57] Claudin-4 (anti-CLDN4, #329400, Invitrogen), mesothelin (anti-MSLN, #354200, Invitrogen), mucin-4 (anti-MUC4, #354900, Invitrogen), and cadherin-11 (anti-CDH11, ab151446, Abcam). Antibodies as supplied (100 μg in 200 μL) were added to a suspension of the QD-FcR complex to give three antibodies per QD and incubated for 1 h at RT.

Characterization of QDs. Absorbance spectra were obtained using a Varian Cary 50 UV/vis spectrophotometer (Agilent Technologies, Santa Clara, CA). For CdSe/(Cd,Zn)S QDs suspended in chloroform it was necessary to dilute the starting solution. Typically, 2 μL QD suspension was added to 700 μL chloroform in a quartz cuvette. For water solubilized QDs, dilution was not necessary and the entire sample was used for absorbance measurements.

The effectiveness of water solubilization was quantitatively determined from the fraction of QDs recovered after filtration through a 200 nm PTFE 13-mm-diameter syringe filter prior to each measurement. The fraction recovered is defined as the number moles of QDs recovered after water solubilization and filtration normalized to the number of moles of QDs in chloroform prior to water solubilization.[27] Particle size distributions and zeta potential were obtained using a Nano Zetasizer (Malvern, Worcestershire, UK) (Supporting Information). Error bars represent standard error.

Cell Culture. Targeting experiments were performed using three pancreatic cancer cell lines: MIA PaCa-2, Panc-1, and Capan-1. The human pancreatic duct epithelium cell line (HPDE) was used as a control. Panc-1 and MIA PaCa-2 cells were cultured using DMEM supplemented with 10% FBS and 1% Pen-strep. Capan-1 cells were cultured using IMDM supplemented with 20% FBS and 1% Pen-strep. HPDE cells were cultured with keratinocyte SFM media supplemented with 0.1 $ng\ mL^{-1}$ of EGF and 30 $\mu g\ mL^{-1}$ of bovine pituitary extract. The passage number for the cells used was as follows: 3−25 (MIA PaCa-2), 3−18 (Panc-1), 3−12 (Capan-1), and 3−10 (HPDE).

Calibration of QD Emission. Stock solutions of QDs in water were prepared with concentrations from 150 nM to 1 nM. 5 μL of the QD suspension was dispensed onto a glass slide. A 22 mm × 22 mm coverslip was placed on top of the drop, which was allowed to spread out to completely contact the coverslip. Fluorescence images were recorded at five random locations using identical conditions as for cell imaging. After subtracting the background, the average intensity was plotted versus the QD concentration per unit area. The QD concentration per unit area was calculated from the volume of the drop, the QD concentration, and area. The calibration curve was then used to convert the fluorescence intensity per unit area on a cell surface to the number of QDs per unit area.

Targeting and Imaging. Cells were grown for 6 to 12 days and were trypsinized at 80−90% confluency. 2 mL of 0.5% trypsin-EDTA was used to lift off cells from the plates. After incubation, 2.5 mL of trypsin inhibitor was used for HPDE cell line. Next, 8 mL of medium was added to the plate to neutralize the trypsin. The cells were then transferred to a 15 mL tube and centrifuged at 1000 rpm for 3 min, and resuspended in 5 mL of medium. The number of cells was determined using a hemocytometer.

5×10^4 cells were seeded in each well (12-well plate) and cultured for 2 days. Cells is each well were washed with PBS once and fixed with 3.7% formaldehyde for 15 min, and then washed again three times with PBS. Cells were blocked with 20% horse serum for 1−2 h and washed three times with PBS. QDs were injected into each well with 500 μL of PBS and incubated for 20 min in room temperature. In experiments to confirm target saturation, the amount of QDs varied from 3×10^6 to 9×10^7 QDs per cell. In all other experiments the QD concentration was 2×10^8 QDs per cell. The cells were then washed with PBS three times. Finally, 1 mL of PBS was added to each well for imaging.

In control experiments, conventional immunofluorescence experiments were performed to image CLDN4, MSLN, MUC4, and CDH11 expression on Panc-1 cells. Briefly, Panc-1 cells were fixed with 3.7% formaldehyde (diluted in PBS buffer) for 15 min and washed 3 times with PBS. Cells were then blocked using 20% horse serum for 1 h prior to incubation with primary antibodies. Claudin-4 was labeled using mouse anti-CLDN4-Alexa Fluor 594 Conjugate (329494, Invitrogen.). The other three proteins were labeled using primary mouse antibodies (aMSLN, aMUC4, and aCDH11) and a secondary goat anti-mouse Alexa Fluor 594 (A-11005, Invitrogen).

Phase and fluorescence images were obtained using a Nikon TE-2000 microscope and analyzed using NIS-elements software with a 20× objective. Using a Nikon DS-Qi1Mc-U3 camera, the pixel size was 0.32 × 0.32 μm. Confocal images were obtained using a Nikon TiE spinning disk microscope. Images were taken in 60−100 z-steps (0.2−0.3 μm per z-step) with a resolution of 0.4 μm/pixel at an exposure time of 200 ms.

Fluorescence intensities of single cells were obtained from NIS element software. The background intensities were recorded from selected regions without cells. After subtracting the background, the fluorescence intensity per unit area on a cell surface was converted to expression level per unit area by using the previously performed calibration curve. Critical steps in the protocols are summarized in Supporting Information.

dx.doi.org/10.1021/bc5003778 | Bioconjugate Chem. 2014, 25, 1893−1901

■ ASSOCIATED CONTENT

Supporting Information

Relative expression levels (where known) for biomarker/cell combinations. Tabulated data for all targeting experiments. Distributions of fluorescence intensity per pixel for claudin-4 (CLDN4), mucin-4 (MUC4), mesothelin (MSLN), and cadherin-11 (CDH11) for single Panc-1 cells. Immunofluorescence control experiments: Panc1 cells incubated with a primary antibody (aCLDN4, aMSLN, aMUC4, and aCDH11) and a fluorescently labeled secondary antibody. QD control experiments: Panc-1 cells incubated with QD-lipid conjugates, QD-NTA/Ni(II) conjugates and QD-FcR-aCLDN4 conjugates, after preincubation with aCLDN4. Schematic illustration of lipid functionalization. Quantitative analysis of negative controls. Critical steps in the protocol. Lipid functionalization of QDs. This material is available free of charge via the Internet at http://pubs.acs.org.

■ AUTHOR INFORMATION

Corresponding Author

*E-mail: searson@jhu.edu.

Notes

The authors declare no competing financial interest.

■ ACKNOWLEDGMENTS

This work was supported by NIH (U54CA151838). K.H.L. acknowledges support from KIST (#2Z04150).

■ REFERENCES

(1) Arruebo, M., Valladares, M., and Gonzalez-Fernandez, A. Antibody-conjugated nanoparticles for biomedical applications, *J. Nanomater.* 2009, DOI: 10.1155/2009/439389.

(2) Niemeyer, C. M. (2001) Nanoparticles, proteins, and nucleic acids: Biotechnology meets materials science. *Angew. Chem., Int. Ed. 40* (22), 4128−4158.

(3) Gomez-Hens, A., Fernandez-Romero, J. M., and Aguilar-Caballos, M. P. (2010) High throughput bioassays using nanoparticles. *Comb. Chem. High Throughput Screening 13* (4), 309−317.

(4) Sanvicens, N., and Marco, M. P. (2008) Multifunctional nanoparticles - properties and prospects for their use in human medicine. *Trends Biotechnol. 26* (8), 425−433.

(5) Chames, P., Van Regenmortel, M., Weiss, E., and Baty, D. (2009) Therapeutic antibodies: successes, limitations and hopes for the future. *Br. J. Pharmacol. 157* (2), 220−233.

(6) Colombo, M., Carregal-Romero, S., Casula, M. F., Gutierrez, L., Morales, M. P., Bohm, I. B., Heverhagen, J. T., Prosperi, D., and Parak, W. J. (2012) Biological applications of magnetic nanoparticles. *Chem. Soc. Rev. 41* (11), 4306−4334.

(7) Petryayeva, E., Algar, W. R., and Medintz, I. L. (2013) Quantum dots in bioanalysis: a review of applications across various platforms for fluorescence spectroscopy and imaging. *Appl. Spectrosc. 67* (3), 215−252.

(8) Allen, T. M. (2002) Ligand-targeted therapeutics in anticancer therapy. *Nat. Rev. Cancer 2* (10), 750−763.

(9) Yu, M. K., Park, J., and Jon, S. (2012) Targeting strategies for multifunctional nanoparticles in cancer imaging and therapy. *Theranostics 2* (1), 3−44.

(10) Davis, M. E., Chen, Z., and Shin, D. M. (2008) Nanoparticle therapeutics: an emerging treatment modality for cancer. *Nat. Rev. Drug Discovery 7* (9), 771−782.

(11) Al-Jamal, W. T., Al-Jamal, K. T., Tian, B., Lacerda, L., Bornans, P. H., Frederik, P. M., and Kostarelos, K. (2008) Lipid-quanturn dot bilayer vesicles enhance tumor cell uptake and retention in vitro and in vivo. *ACS Nano 2* (3), 408−418.

(12) Bruchez, M. P. (2011) Quantum dots find their stride in single molecule tracking. *Curr. Opin. Chem. Biol. 15* (6), 775−780.

(13) Jin, T., Tiwari, D. K., Tanaka, S., Inouye, Y., Yoshizawa, K., and Watanabe, T. M. (2010) Antibody-ProteinA conjugated quantum dots for multiplexed imaging of surface receptors in living cells. *Mol. Biosyst. 6* (11), 2325−2331.

(14) Zrazhevskiy, P.; Gao, X. H. Quantum dot imaging platform for single-cell molecular profiling. *Nat. Commun.* 2013, *4*.

(15) You, C., Bhagawati, M., Brecht, A., and Piehler, J. (2009) Affinity capturing for targeting proteins into micro and nanostructures. *Anal. Bioanal. Chem. 393* (6−7), 1563−1570.

(16) Lee, K. H., Galloway, J. F., Park, J., Dvoracek, C. M., Dallas, M., Konstantopoulos, K., Maitra, A., and Searson, P. C. (2012) Quantitative molecular profiling of biomarkers for pancreatic cancer with functionalized quantum dots. *Nanomedicine 8* (7), 1043−51.

(17) Nimmerjahn, F., and Ravetch, J. V. (2008) Fc gamma receptors as regulators of immune responses. *Nat. Rev. Immunol. 8* (1), 34−47.

(18) Woof, J. M., and Burton, D. R. (2004) Human antibody-Fc receptor interactions illuminated by crystal structures. *Nat. Rev. Immunol. 4* (2), 89−99.

(19) Takai, T. (2002) Roles of Fc receptors in autoimmunity. *Nat. Rev. Immunol. 2* (8), 580−592.

(20) Daeron, M. (1997) Fc receptor biology. *Annu. Rev. Immunol. 15*, 203−34.

(21) Ravetch, J. V., and Bolland, S. (2001) IgG Fc receptors. *Annu. Rev. Immunol. 19*, 275−290.

(22) Akerstrom, B., Nielsen, E., and Bjorck, L. (1987) Definition of Igg-binding and albumin-binding regions of streptococcal protein-G. *J. Biol. Chem. 262* (28), 13388−13391.

(23) Surolia, A., Pain, D., and Khan, M. I. (1982) Protein-a - natures universal anti-antibody. *Trends Biochem. Sci. 7* (2), 74−76.

(24) Eliasson, M., Olsson, A., Palmcrantz, E., Wiberg, K., Inganas, M., Guss, B., Lindberg, M., and Uhlen, M. (1988) Chimeric IgG-binding receptors engineered from staphylococcal protein-A and streptococcal protein-G. *J. Biol. Chem. 263* (9), 4323−4327.

(25) Knecht, S., Ricklin, D., Eberle, A. N., and Ernst, B. (2009) Oligohis-tags: mechanisms of binding to Ni(II)-NTA surfaces. *J. Mol. Recognit. 22* (4), 270−279.

(26) Dill, K., Lin, M., Poteras, C., Fraser, C., Hafeman, D. G., Owicki, J. C., and Olson, J. D. (1994) Antibody-antigen binding constants determined in solution-phase with the threshold membrane-capture system - binding constants for antifluorescein, anti-saxitoxin, and anti-ricin antibodies. *Anal. Biochem. 217* (1), 128−138.

(27) Galloway, J. F., Winter, A., Lee, K. H., Park, J. H., Dvoracek, C. M., Devreotes, P., and Searson, P. C. (2012) Quantitative characterization of the lipid encapsulation of quantum dots for biomedical applications. *Nanomedicine 8* (7), 1190−9.

(28) van Schooneveld, M. M., Vucic, E., Koole, R., Zhou, Y., Stocks, J., Cormode, D. P., Tang, C. Y., Gordon, R. E., Nicolay, K., Meijerink, A., Fayad, Z. A., and Mulder, W. J. M. (2008) Improved biocompatibility and pharmacokinetics of silica nanoparticles by means of a lipid coating: A multimodality investigation. *Nano Lett. 8* (8), 2517−2525.

(29) Carion, O., Mahler, B., Pons, T., and Dubertret, B. (2007) Synthesis, encapsulation, purification and coupling of single quantum dots in phospholipid micelles for their use in cellular and in vivo imaging. *Nat. Protoc. 2* (10), 2383−2390.

(30) Danielsson, A., Ljunglof, A., and Lindblom, H. (1988) One-step purification of monoclonal IgG antibodies from mouse ascites. An evaluation of different adsorption techniques using high performance liquid chromatography. *J. Immunol. Methods 115* (1), 79−88.

(31) Lata, S., Reichel, A., Brock, R., Tampe, R., and Piehler, J. (2005) High-affinity adaptors for switchable recognition of histidine-tagged proteins. *J. Am. Chem. Soc. 127* (29), 10205−10215.

(32) Huang, Z. H., Park, J. I., Watson, D. S., Hwang, P., and Szoka, F. C. (2006) Facile synthesis of multivalent nitrilotriacetic acid (NTA) and NTA conjugates for analytical and drug delivery applications. *Bioconjugate Chem. 17* (6), 1592−1600.

(33) Yunis, A. A., Arimura, G. K., and Russin, D. J. (1977) Human pancreatic carcinoma (MIA PaCa-2) in continuous culture: sensitivity to asparaginase. *Int. J. Cancer 19* (1), 128−35.
(34) Tan, M. H., Nowak, N. J., Loor, R., Ochi, H., Sandberg, A. A., Lopez, C., Pickren, J. W., Berjian, R., Douglass, H. O., Jr., and Chu, T. M. (1986) Characterization of a new primary human pancreatic tumor line. *Cancer Invest. 4* (1), 15−23.
(35) Lieber, M., Mazzetta, J., Nelson-Rees, W., Kaplan, M., and Todaro, G. (1975) Establishment of a continuous tumor-cell line (panc-1) from a human carcinoma of the exocrine pancreas. *Int. J. Cancer 15* (5), 741−7.
(36) Fogh, J., Fogh, J. M., and Orfeo, T. (1977) 127 Cultured human tumor-cell lines producing tumors in nude mice. *J. Natl. Cancer I 59* (1), 221−226.
(37) Liu, N., Furukawa, T., Kobari, M., and Tsao, M. S. (1998) Comparative phenotypic studies of duct epithelial cell lines derived from normal human pancreas and pancreatic carcinoma. *Am. J. Pathol. 153* (1), 263−269.
(38) Michl, P., Buchholz, M., Rolke, M., Kunsch, S., Lohr, M., McClane, B., Tsukita, S., Leder, G., Adler, G., and Gress, T. M. (2001) Claudin-4: A new target for pancreatic cancer treatment using Clostridium perfringens enterotoxin. *Gastroenterology 121* (3), 678−684.
(39) Li, M., Bharadwaj, U., Zhang, R. X., Zhang, S., Mu, H., Fisher, W. E., Brunicardi, F. C., Chen, C. Y., and Yao, Q. Z. (2008) Mesothelin is a malignant factor and therapeutic vaccine target for pancreatic cancer. *Mol. Cancer Ther. 7* (2), 286−296.
(40) Argani, P., Iacobuzio-Donahue, C., Ryu, B., Rosty, C., Goggins, M., Wilentz, R. E., Murugesan, S. R., Leach, S. D., Jaffee, E., Yeo, C. J., Cameron, J. L., Kern, S. E., and Hruban, R. H. (2001) Mesothelin is overexpressed in the vast majority of ductal adenocarcinomas of the pancreas: Identification of a new pancreatic cancer marker by serial analysis of gene expression (SAGE). *Clin. Cancer Res. 7* (12), 3862−3868.
(41) Andrianifahanana, M., Moniaux, N., Schmied, B. M., Ringel, J., Friess, H., Hollingsworth, M. A., Buchler, M. W., Aubert, J. P., and Batra, S. K. (2001) Mucin (Muc) gene expression in human pancreatic adenocarcinoma and chronic pancreatitis: a potential role of Muc4 as a tumor marker of diagnostic significance. *Clin. Cancer Res. 7* (12), 4033−4040.
(42) Singh, A. P., Chauhan, S. C., Andrianifahanana, M., Moniaux, N., Meza, J. L., Copin, M. C., van Seuningen, I., Hollingsworth, M. A., Aubert, J. P., and Batra, S. K. (2007) MUC4 expression is regulated by cystic fibrosis transmembrane conductance regulator in pancreatic adenocarcinoma cells via transcriptional and post-translational mechanisms. *Oncogene 26* (1), 30−41.
(43) Hewitt, K. J., Agarwal, R., and Morin, P. J. (2006) The claudin gene family: expression in normal and neoplastic tissues. *BMC Cancer 6* (186), 1−8.
(44) Nichols, L. S., Ashfaq, R., and Iacobuzio-Donahue, C. A. (2004) Claudin 4 protein expression in primary and metastatic pancreatic cancer - Support for use as a therapeutic target. *Am. J. Clin. Pathol. 121* (2), 226−230.
(45) Foss, C. A., Fox, J. J., Feldmann, G., Maitra, A., Iacobuzio-Donohue, C., Kern, S. E., Hruban, R., and Pomper, M. G. (2007) Radiolabeled anti-claudin 4 and anti-prostate stem cell antigen: Initial imaging in experimental models of pancreatic cancer. *Mol. Imaging 6* (2), 131−139.
(46) Ueda, J., Semba, S., Chiba, H., Sawada, N., Seo, Y., Kasuga, M., and Yokozaki, H. (2007) Heterogeneous expression of claudin-4 in human colorectal cancer: Decreased claudin-4 expression at the invasive front correlates cancer invasion and metastasis. *Pathobiology 74* (1), 32−41.
(47) Michl, P., Buchholz, M., Rolke, M., Kunsch, S., Lohr, M., Adler, G., and Gress, T. M. (2002) Functional characterization of claudin-4 in pancreatic cancer cells. *Gastroenterology 122* (4), A492−A492.
(48) Maitra, A., Adsay, N. V., Argani, P., Iacobuzio-Donahue, C., De Marzo, A., Cameron, J. L., Yeo, C. J., and Hruban, R. H. (2003) Multicomponent analysis of the pancreatic adenocarcinoma progression model using a pancreatic intraepithelial neoplasia tissue microarray. *Mod. Pathol. 16* (9), 902−912.
(49) Hassan, R., Laszik, Z. G., Lerner, M., Raffeld, M., Postier, R., and Brackett, D. (2005) Mesothelin is overexpressed in pancreaticobiliary adenocarcinomas but not in normal pancreas and chronic pancreatitis. *Am. J. Clin. Pathol. 124* (6), 838−45.
(50) Alameda, F., Mejias-Luque, R., Garrido, M., and de Bolos, C. (2007) Mucin genes (MUC2, MUC4, MUC5AC, and MUC6) detection in normal and pathological endometrial tissues. *Int. J. Gynecol. Pathol. 26* (1), 61−5.
(51) Chaturvedi, P., Singh, A. P., Moniaux, N., Senapati, S., Chakraborty, S., Meza, J. L., and Batra, S. K. (2007) MUC4 mucin potentiates pancreatic tumor cell proliferation, survival, and invasive properties and interferes with its interaction to extracellular matrix proteins. *Mol. Cancer Res. 5* (4), 309−320.
(52) Binkley, C. E., Zhang, L., Greenson, J. K., Giordano, T. J., Kuick, R., Misek, D., Hanash, S., Logsdon, C. D., and Simeone, D. M. (2004) The molecular basis of pancreatic fibrosis: common stromal gene expression in chronic pancreatitis and pancreatic adenocarcinoma. *Pancreas 29* (4), 254−63.
(53) Iacobuzio-Donahue, C. A., Maitra, A., Shen-Ong, G. L., van Heek, T., Ashfaq, R., Meyer, R., Walter, K., Berg, K., Hollingsworth, M. A., Cameron, J. L., Yeo, C. J., Kern, S. E., Goggins, M., and Hruban, R. H. (2002) Discovery of novel tumor markers of pancreatic cancer using global gene expression technology. *Am. J. Pathol. 160* (4), 1239−49.
(54) Logsdon, C. D., Simeone, D. M., Binkley, C., Arumugam, T., Greenson, J. K., Giordano, T. J., Misek, D. E., Kuick, R., and Hanash, S. (2003) Molecular profiling of pancreatic adenocarcinoma and chronic pancreatitis identifies multiple genes differentially regulated in pancreatic cancer. *Cancer Res. 63* (10), 2649−57.
(55) Sipos, B., Moser, S., Kalthoff, H., Torok, V., Lohr, M., and Kloppel, G. (2003) A comprehensive characterization of pancreatic ductal carcinoma cell lines: towards the establishment of an in vitro research platform. *Virchows Arch. 442* (5), 444−52.
(56) Park, J., Lee, K. H., Galloway, J. F., and Searson, P. C. (2008) Synthesis of cadmium selenide quantum dots from a non-coordinating solvent: growth kinetics and particle size distribution. *J. Phys. Chem. C 112* (46), 17849−17854.
(57) Harsha, H. C., Kandasamy, K., Ranganathan, P., Rani, S., Ramabadran, S., Gollapudi, S., Balakrishnan, L., Dwivedi, S. B., Telikicherla, D., Selvan, L. D. N., Goel, R., Mathivanan, S., Marimuthu, A., Kashyap, M., Vizza, R. F., Mayer, R. J., DeCaprio, J. A., Srivastava, S., Hanash, S. M., Hruban, R. H., and Pandey, A. (2009) A compendium of potential biomarkers of pancreatic cancer. *Plos Med. 6* (4), e1000046.